Indonesian Journal of Aerospace Vol. 24 No. 1 Juni 2026 : pp 1–16 (Pratomo et al.)
DOI: 10.55981/ijoa.2026.15829
https://ejournal.brin.go.id/ijoa/

Evaluation of Adhesive Joint Performance in Aluminum Single-Lap Joints Using Experiments and FEA.

Rezky Agung Pratomo[1], Kosim Abdurohman[2], Riki Ardiansyah[2], Afid Nugroho[2], Fajar Ari Wandono[2], Awang Rahmadi Nuranto[2], Mochamad Chalid[1*]

[1] Department of Metallurgical and Materials Engineering, Faculty of Engineering, Universitas Indonesia, Depok 16424, West Java, Indonesia
[2]Research Center for Aeronautics Technology, National Research and Innovation Agency, 16350 Jawa Barat, Indonesia
*e-mail: m.chalid@ui.ac.id

Received: 19/03/2026 Revised: 28/04/2026 Accepted: 4/05/2026. Published: 26/10/2026

Abstract

In order to assess adhesive performance, this work employed numerical simulations, single lap joint (SLJ) testing, and material characterization. Three different types of glue were analyzed for their mechanical behavior and joint performance. ASTM D638 was first used to evaluate the general adhesive qualities' elastic modulus, strength, and ductility. In accordance with ASTM D5868, tensile testing was employed to evaluate the bonded SLJ's structural performance. Finally, a simplified finite element analysis (FEA) model based on springs was developed to investigate stress distribution in more detail. The results showed significant variations in the mechanical response: high-modulus adhesives demonstrated better stiffness but lower strain capacity, while more ductile adhesives demonstrated lower strength. These experimental results demonstrate that the adhesive selection significantly affects the shear strength, deformation behavior, and failure mechanism of the overlap joint. The strongest junction was created by the adhesive with the highest modulus of elasticity; adhesives with lower moduli had a larger capacity for deformation but less strength. In accordance with conventional joint theory, modeling findings showed that shear stress was concentrated at the borders of the overlap area and decreased toward the center. Examining theoretical, experimental, and numerical findings reveals good agreement; the differences between the theoretical predictions and the simulation and experimental results are 5.59% and 1.51%, respectively. In summary, this study highlights the relationship between adhesive properties and joint performance and shows how simplified numerical models may precisely forecast the mechanical behavior and stress distribution in adhesive-bonded SLJ joints.

Keywords: Adhesive, Finite Element Analysis, Shear Strength, Single Lap Joint, Viscosity.

Nomenclature

A_a	=	adhesive area, m^2	K_{si}	=	internal element shear stiffness
D	=	distance between grips rigid, mm	L	=	length of narrow section, mm
E	=	adhesive modulus of elasticity, Pa	n	=	thickness of adhesive
F	=	force, N	R	=	rigid plastic fillet radius, mm
$f_{x,i}$	=	spring force x direction at node i	T	=	rigid plastic thickness, mm
$f_{y,i}$	=	spring force y direction at node i	τ_i	=	shear stress at node i
G	=	shear modulus of adhesive, Pa	τ_{avg}	=	average shear stress
G_l	=	gauge length parameter, mm	τ_a	=	adhesive layer thickness, mm
K_{se}	=	edge element shear stiffness	W	=	a narrow strip of rigid plastic, mm
K_{sc}	=	corner element shear stiffness	W_0	=	overall width rigid plastic, mm

e-ISSN 2597-7873 (online) | © 2026 The Author(s). Published by BRIN Publishing.
This is an open access article under the CC BY-SA license(https://creativecommons.org/licenses/by-sa/4.0/)
IJOA accredited as Sinta 2 Journal (https://sinta.kemdikbud.go.id/journals/profile/3362)

1. Introduction

The automotive, motorcycle, and aerospace industries have experienced remarkable growth over the past decade, driving the development of lightweight, energy-efficient structures manufactured from a combination of advanced engineering materials. The usage of lightweight materials including aluminum, magnesium, and fiber-reinforced polymer (FRP) composites has increased due to stricter restrictions concerning crashworthiness, fuel economy, and greenhouse gas emissions. (Dachev, Kazilas, Alfano, & Omairey, 2025; Wei, Jin, Luo, Li, & Sun, 2024). However, using many materials into a single structure presents significant joining challenges. Conventional joining techniques like welding and mechanical fastening are often inappropriate for multi-material assemblies because they can lead to localized weakening, promote galvanic corrosion between dissimilar metals, and create high stress concentrations around the joint, ultimately compromising structural performance (Cui, Tian, Wang, & Dong, 2021; Maggiore, Banea, Stagnaro, & Luciano, 2021). In order to get over these limitations, adhesive bonding has emerged as a successful alternative connection method. Adhesive bonding, as opposed to conventional connecting methods, increases fatigue resistance, lowers overall weight, and more evenly distributes stresses across the bonded surface. Because of these advantages, adhesive joints are particularly desirable for electric vehicle (EV) applications, such as battery enclosures and vehicle body components. (Hecht, Fass, & Baumgartner, 2023; Ramaswamy, O'Higgins, Kadiyala, McCarthy, & McCarthy, 2020). Additionally, by eliminating the need for drilling or welding, adhesive bonding maintains the integrity of substrates with thin walls or layers. Additionally, adhesive joints provide excellent vibration damping, greater design freedom, and improved corrosion resistance. These characteristics make adhesive bonding one of the most promising joining technologies for automotive and aerospace applications. (Marchione, 2020; Teixeira de Freitas & Sinke, 2015). As a result, several sectors now favor adhesive bonding as a joining method.

The mechanical performance of adhesive connections has been thoroughly studied in the past by looking at variables such adhesive thickness, overlap geometry, and surface treatment (Rahul, Suresh, Narendran, & Haribaskar, 2023; Wu et al., 2016; D. Zhang & Huang, 2021). Because it directly affects the quality of adhesion between the adhesive and the substrate, surface preparation is one of these factors. For instance, it has been shown that adding controlled surface roughness greatly increases the lap shear strength of bonded aluminum joints (L. Guo et al., 2021). Similarly, overlap length and adhesive thickness have an impact on the distribution of stress in the bonded area, which in turn affects the joint's ability to support loads (Vinay, 2021). By adding adhesive fillets along the joint edges, which have been demonstrated to boost the load-bearing capacity by over 50%, stress concentrations can be further reduced (Akpinar, Doru, Özel, Aydin, & Jahanpasand, 2013). Because they increase surface wettability and foster greater adherence at the adhesive–substrate interface, sophisticated surface treatments like laser texturing and micro-patterning have garnered a lot of interest more lately (Andarabi, Shelesh-Nezhad, & Chakherlou, 2022).

The majority of these studies have concentrated on improving specific parameters while using only one adhesive system, despite the fact that they have greatly increased our understanding of adhesive joint behavior. As a result, there are still few direct comparisons of structural adhesives with significantly varied mechanical properties, especially aerospace-grade and non-aerospace-grade adhesives. Similarly, numerical studies using Cohesive Zone Models (CZM) have yielded important information about the beginning of damage and the progression of failure. However, there has not been much focus on experimentally verified simpler finite element models, particularly for aluminum adhesive joints (Marchione, 2023; Moazzami et al., 2023).

Depending on their intended uses, structural adhesives have a wide range of mechanical properties. Aerospace-grade adhesives, such as 3MTM Scotch-WeldTM EC-2216 B/A and Araldite® 420A, are typically designed to offer enhanced cohesive strength, high stiffness, and exceptional temperature resistance. On the other hand, industrial methacrylate adhesives like Crestabond® M1-20 are appealing for high-volume manufacturing applications because of their increased durability, quicker curing periods, and simpler processing.(Paz, Narbón, Abenojar, Cledera, & del Real, 2016). Despite these differences, systematic evaluations under identical specimen geometries, loading conditions, and curing procedures remain limited.

To close this research gap, an experimental and statistical comparison is made between the performance of two aerospace-grade adhesives (Araldite® 420A and 3MTM Scotch-Weld TM EC-2216 B/A) and one non-aerospace-grade adhesive (Crestabond® M1-20) in aluminum single-lap joints. Tensile and lap shear testing were used to assess the mechanical properties and failure behavior of each adhesive system, and simplified finite element models were developed to support the experimental results. In automotive and aerospace applications, where finding the ideal balance between toughness, stiffness, and manufacturing economy is essential, the results provide helpful suggestions for selecting structural adhesives.

2. Methodology

2.1. Material

The adherend used is Aluminum (Al) type (5058). Aluminum (Al) alloys in the 5xxx family are wrought alloys that do not require heat treatment and are frequently used in transportation and maritime applications. Due to their excellent corrosion resistance and weldability (C. Guo et al., 2023; R. Zhang et al., 2019). The adherends were made by cutting aluminum plates according to the dimension ASTM D5868 using a water jet. Adherend specimens were machined to a thickness of 2 mm, a length of 101.6 mm (4 in.), and a width of 25.4 mm (1 in). There are 30 adherends made from aluminum plates, which will be made into specimens for every two adherends. Furthermore, each sample SLJ contain of 5 specimens. Each adherend receives abrasive treatment using sandpaper 800 on the adhesive overlap surface. After completing the abrasive surface treatment, the contact angle of the adherend surface was evaluated with a VHX-5000 digital microscope at the Advanced Physics Imaging Laboratory, BRIN, as illustrated in Figure 2.1. According to prior research, employing sandpaper belts of different grit sizes for surface preparation in the joint area can greatly improve adhesion performance (Abdurohman et al., 2024). Therefore, this method is employed.



Figure 2.1: The VHX-5000 Digital Microscope for Contact Angle.

Tabs for the specimens were produced from Glass Fiber Reinforced Polymer (GFRP) composite via the Vacuum-Assisted Resin Infusion (VARI) process. Each specimen was fitted

with a pair of 25.4 mm × 25.4 mm tabs, attached symmetrically to both ends, as illustrated in Figure 2.2.

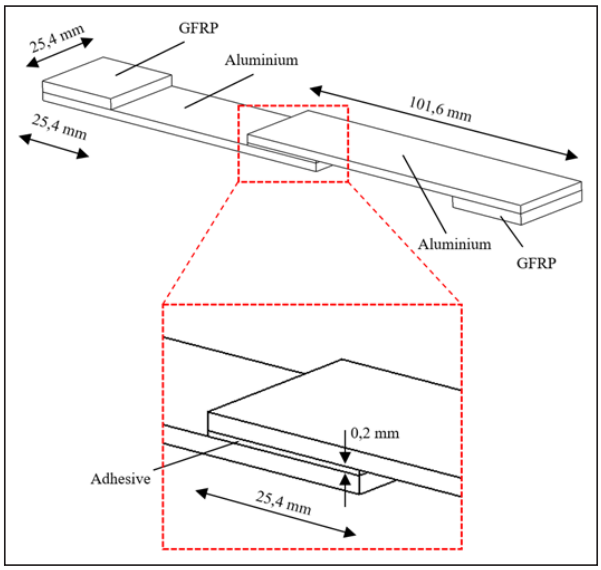


Figure 2.2: SLJ Specimen Dimension.

The three types of adhesives used are 3M™ Scotch-Weld™ EC-2216 B/A epoxy adhesive (A1), Aerospace Adhesives Araldite ® 420 A (A2) and Crestabond M1-20 (A3). Three adhesives were selected to evaluate the performance differences between aerospace-grade and non-aerospace-grade adhesives available in the laboratory. Adhesives A1 and A2 are classified as aerospace-grade, while adhesive A3 is a non-aerospace-grade adhesive. There are 15 adhesives created using molding based on the ASTM D638 guideline, as shown in Figure 2.3. Each sample (A1, A2, and A3) cont ıs of 5 adhesive specimens. The specir geometry consists of th llowing dimensions: L_0= 165 mm, D = 115 mm, L = 57 mm, G_lG_l= 50 mm, W = 13 mm, W_0=19 mm, T = 7 mm, and R = 76 mm.

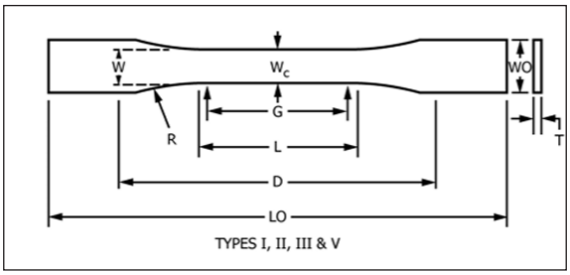


Figure 2.3: Adhesive Specimen Dimension (ASTM International, 2014).

Understanding the performance characteristics of each adhesive allows for more precise selection based on structural requirements. Adhesives with lower strength can be applied to structures with minimal joint strength demands, whereas higher-strength adhesives can be utilized for structures requiring enhanced joint performance. The adhesive used in the study, shown in Table 2-1 contains the following parameters.

Table 2-1: Technical Data Sheet of Adhesive

Adhesive	Viscosity (Pa.s)	Gel time (s)
A1	86.25	5400
A2	40	3600
A3	110	900-1320

2.2. Experimental

2.2.1. Tensile Test of Adhesive Material

To determine the adhesive's elastic modulus and single-lap shear test, the experiments took place at the Materials Testing Laboratory of the Research Center for Aeronautics Technology, ORPA–BRIN, utilizing a 100 kN Tensilon Universal Testing Machine (UTM). Tensile tests are performed on each adhesive substance. Furthermore, for adhesive sample is shown in Figure 2.4, the tensile test was performed at a crosshead speed of 50 mm/min. Elastic modulus is used as input for a single lap joint tensile simulation. The simulation results are used as a comparison with the experimental results.

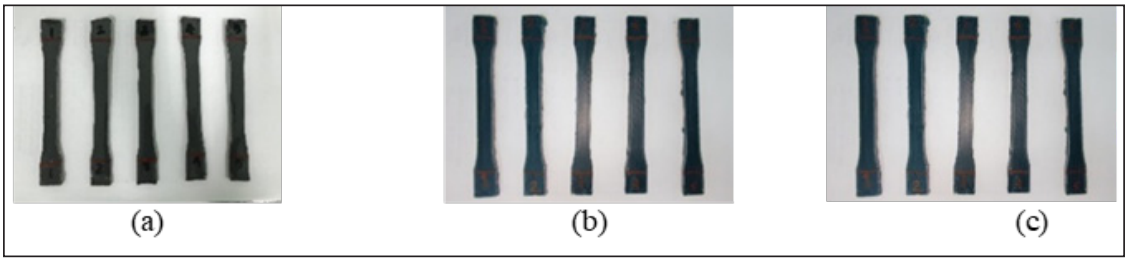


Figure 2.4: Adhesive Specimen (a). A1, (b). A2, (c). A3.

2.2.2. Single-Lap Joint Test

Single-lap shear tests were conducted to evaluate the maximum load that the aluminum joints could withstand. Universal testing machine (UTM) operating at a constant crosshead speed of 13 mm/min, following the ASTM D5868 standard. During testing, each specimen was secured on the UTM by clamping the tabs at both the upper and lower grips, and loading was applied until joint failure or complete separation occurred. The applied load and corresponding shear strength were automatically recorded through the UTM data acquisition system. The testing configuration for the single-lap joint specimens is shown in Figure 2.5. For both the adherend and adhesive tests, the data were obtained by calculating the mean value of one sample set, where each sample set consisted of five specimens.



Figure 2.5: SLJ Specimen on UTM.

2.3. Simulation

To determine the shear stress distribution on the adhesive in a single lap joint, finite element analysis (FEA) is carried out. The adherend (aluminum) is modeled using 2D plane stress elements, while the adhesive is represented by spring elements in the overlap area is shown in Figure 2.6. Tahmasebi initially introduced this adhesive modeling approach to analyze bonded joints (Tahmasebi, 2002). The sticky layer was represented in the simulation as a linear elastic substance. Rigid body elements (RBE) were used to connect spring elements, which were positioned in the middle of the two adherends. Two spring elements that supply stiffness components in both the x and y axes are present in every node in the overlap region. This configuration enables us to examine the distribution of shear stress in a single-lap junction and characterizes the mechanical reaction of the adhesive. The loading parameters and boundary conditions entered are meticulously matched to the first experimental test settings on the UTM. This ensures that the numerical model accurately reflects the physical test conditions an al s e behavior of the joint under load to be evaluated. The shear spring constants ($\boldsymbol{K_{si}}$, $\boldsymbol{K_{se}}$, $\boldsymbol{K_{sc}}$) are shown below.

$$k_{si} = 2k_{se} = 4k_{sc} = \frac{A_a\, G}{t_a} \tag{2-1}$$

The shear stress in an adhesive joint can be determined using the equation given below.

$$\tau_i = \frac{\sqrt{{f_{x,i}}^2 + {f_{y,i}}^2}}{A_a} \tag{2-2}$$

3. The calculation of the average shear stress in the overlap region, derived from the shear stresses at various nodal points, is performed using the following equation.

$$\tau_{avg} = \frac{1}{n}\sum_{i=1}^{n} \tau_i \tag{2-3}$$

The average shear stress acting on the overlap area under load is given by the formula below.

$$\tau_{avg} = \frac{F}{A} \tag{2-4}$$

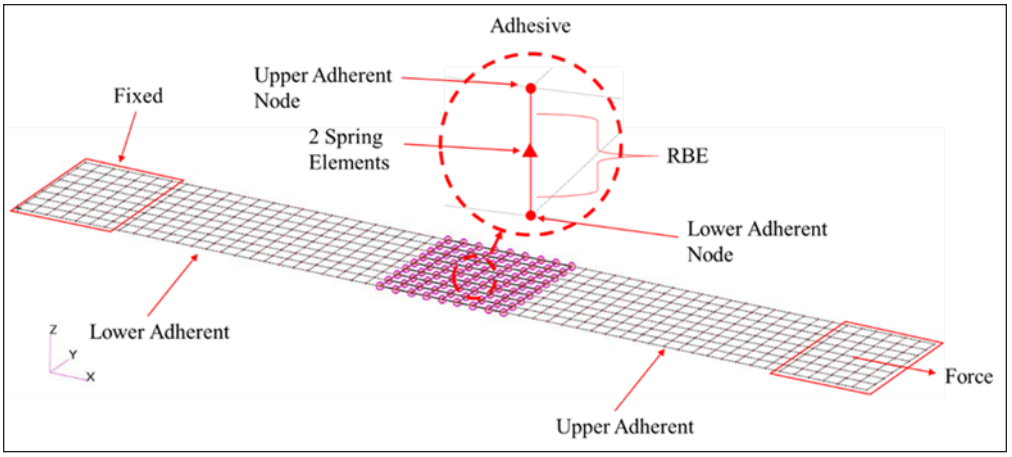


Figure 2.6: Finite element model of the single lap joint.

3. Result and Analysis

3.1. Surface Treatment

Surface morphology was found to significantly affect the quality of the adhesive bond. Contact angle measurements, as shown in Figure 3.1, were conducted to demonstrate the occurrence of a decrease in the contact angle. The contact angle, which was initially 81° at t = 1 s, decreased to 76° at t = 300 s. This is consistent with previous research by experts showing that sanding can reduce the contact angle, increase absorption, and result in an increase in the shear strength of single-lap joints (Boutar, Naïmi, Mezlini, & Ali, 2016). Well, it turns out that a smoother substrate surface can minimize friction and trapped air, making it easier for the adhesive to spread and potentially increasing its bond strength. It turns out that this finding is consistent with the findings of other researchers (L. Guo et al., 2021; D. Zhang & Huang, 2021), They reported that roughening the substrate surface can increase the shear strength of lap joints and make wetting performance more reliable. These points shed light on the fact that surface preparation plays a crucial role in achieving high-quality adhesive bonds.

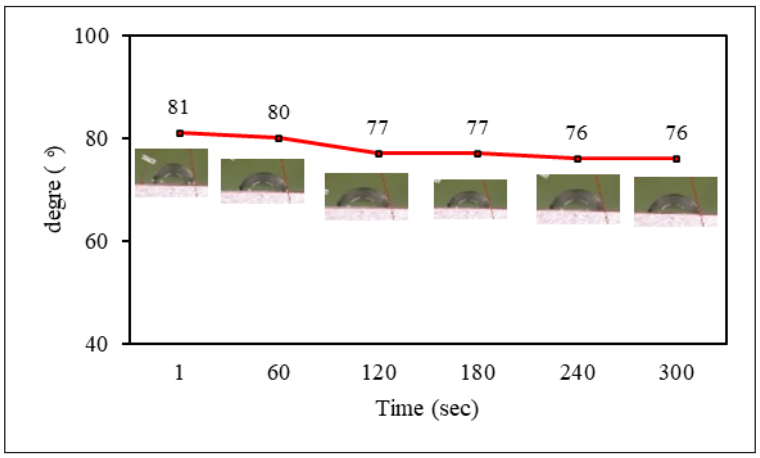


Figure 3.1: Adherend contact angle.

3.2. Adhesive

The stress-strain curves of three different adhesives are displayed in Figure 3.2. The stress-strain curve of an adhesive is a crucial characteristic that is highly helpful for assessing its mechanical performance (Demiral, 2025). Adhesive A2 shows extremely high rigidity in this instance. At a strain of roughly 2%, it reaches a maximum stress of 28 MPa and has a very steep starting slope. High stiffness and quick failure are indicated by this. Adhesive A1, on the other hand, shows neither high nor low stiffness, with a more progressive development in stress that peaks at 10 MPa at a strain of roughly 30%, indicating an ideal ratio of ductility to strength. Lastly, Adhesive A3 has the lowest stiffness, with a high strain capacity (over 40%) and a very low maximum stress (around 0.16 MPa), suggesting strong ductility but low strength. This comparison makes it quite clear that each glue has unique mechanical qualities. A2 is the least ductile but the strongest and stiffest. While A3 is the most ductile but the weakest, A1 provides a balance between strength and ductility. The test's findings support earlier studies' findings that epoxy adhesives are often stronger than acrylic adhesives (Wei et al., 2024). When choosing adhesives for structural applications, where a compromise between strength and flexibility is necessary, this feature has shown to be crucial to take into account.

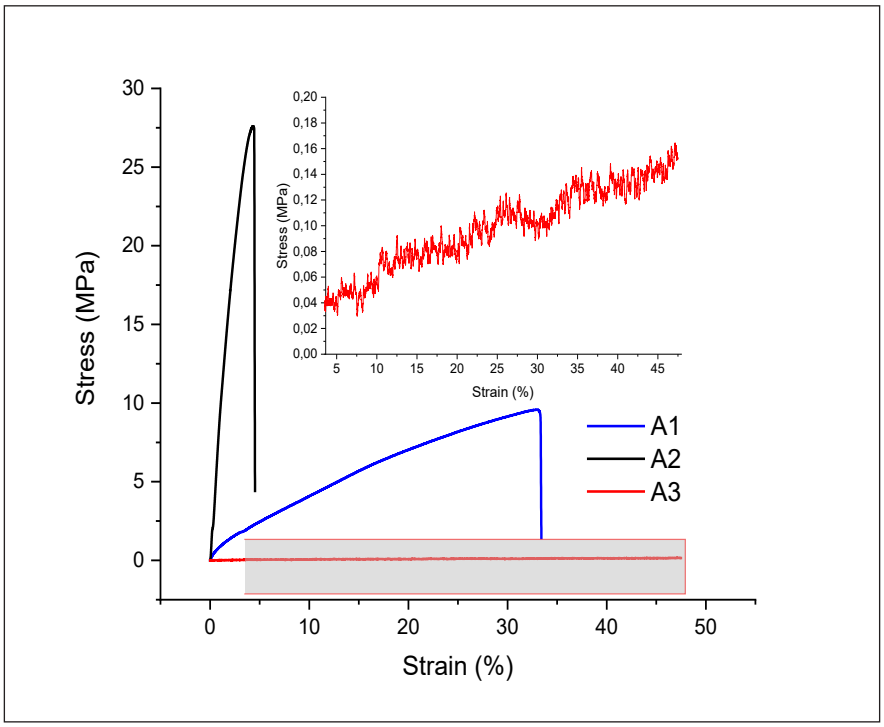


Figure 3.2: Adhesive stress-strain curve.

Figure 3.5 shows the stress-strain relationship for SLJ specimens bonded using three different types of adhesives: A1, A2, and A3. Among the three, SLJ-A2 exhibited the highest lap shear strength of 9.44 ± 0.28 MPa at a strain of approximately 2%. This value indicates a strong but brittle material with minimal deformation prior to failure. Meanwhile, SLJ-A1 achieved an overlap shear strength of 5.1 ± 0.88 MPa at a strain of approximately 1.6%, indicating a balance between stiffness and ductility. In contrast, SLJ-A3 exhibited the lowest shear overlap strength of 4.21 ± 0.62 MPa and failed at a strain of approximately 1.8%. This indicates slightly higher ductility than SLJ-A1 but lower overall strength. (Miturska-Barańska & Rudawska, 2022).

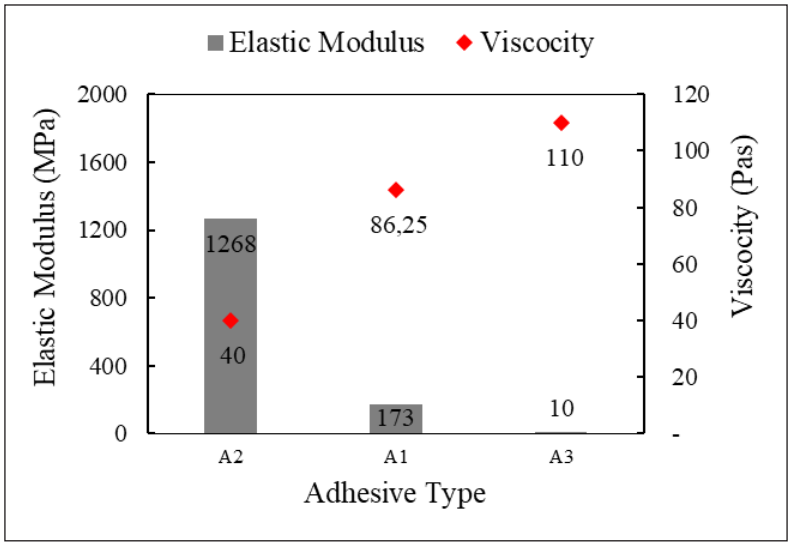


Figure 3.3: Adhesive elastic modulus & viscosity.

3.3. Single Lap Joint

The load-displacement curve of the SLJ specimen is presented in Figure 3.4, whereas the corresponding stress–strain relationship is illustrated in Figure 3.5. The stress-strain curve was derived by recalculating the load and displacement data. Stress was calculated by dividing the applied load by the overlap area of the joint, whereas strain was obtained by dividing the measured displacement by the gauge length. Before testing, both the overlap area (defined by its length and width) and the gauge length were entered into the UTM software, allowing the stress–strain data to be automatically computed throughout the testing process. A2 is an adhesive that has the highest elastic modulus, highest lap shear strength and deformation resistance compared to all the adhesives tested. The lap shear strength of SLJ-A2 reaches 9.44 ± 0.28 MPa at a load of 6000 N and is fractured after 2.9 mm of deformation. Following SLJ-A2 in order of preference are SLJ-A1 and SLJ-A3.

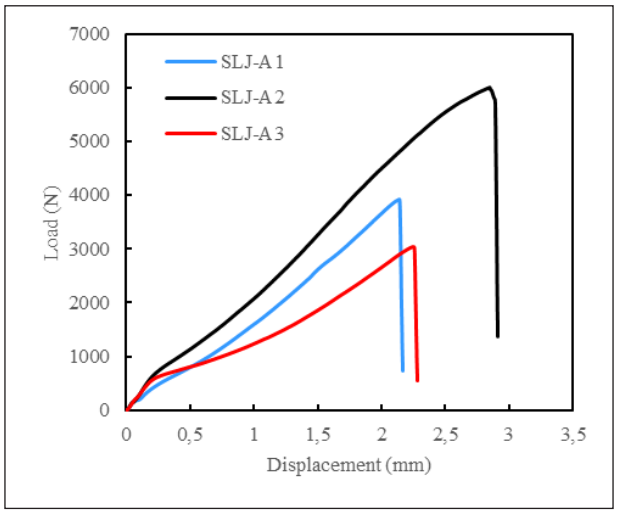


Figure 3.4: Load-Displacement Curve of SLJ Specimens.

Building upon the load-displacement behavior discussed in the previous section, this part details the derived mechanical parameters, specifically the shear strength and elastic modulus of the three SLJ. A summary of these calculated values is presented in Table 3-1, as detailed more extensively in the Figure 3.5.

Table 3-1: Shear Stress and Elastic Modulus SLJ

SLJ	Shear Stress (MPa)	Elastic Modulus (GPa)
SLJ-A1	5.1 ± 0.88	0.3 ± 0.1
SLJ-A2	9.44 ± 0.28	0.77 ± 0.2
SLJ-A3	4.21 ± 0.62	0.53 ± 0.1

The stress-strain relationship for SLJ specimens bound with A1, A2, and A3 adhesives is depicted in Figure 3.5. At a strain of about 2%, SLJ-A2 showed the highest lap shear strength of 9.44 ± 0.28 MPa out of the three. This number denotes a material that is strong but brittle and deforms very little before failing. SLJ-A1, on the other hand, demonstrated a balance between stiffness and ductility with an overlap shear strength of 5.1 ± 0.88 MPa at a strain of roughly 1.6%. On the other hand, SLJ-A3 failed at a strain of about 1.8% and had

the lowest shear overlap strength of 4.21 ± 0.62 MPa. This suggests that overall strength is lower but ductility is somewhat higher than SLJ-A1.

In terms of percentage lap shear strength, SLJ-A2 outperforms the other adhesives by a significant margin, with nearly double the strength of SLJ-A1 and SLJ-A3. The strain at maximum strength for SLJ-A2 is 2%, whereas for SLJ-A1 and SLJ-A3, it is 1.6% and 1.8%, respectively. This investigation emphasizes both SLJ-A2's improved mechanical performance in terms of shear strength and brittleness. The strengths of SLJ-A3 and SLJ-A1 are almost equal: 4.21 ± 0.62 MPa and 5.1 ± 0.88 MPa for lap shear stress, 3041 N and 3922 N for peak load, and fractured at 2.4 mm and 2.2 mm. SLJ-A1 lap shear strength is somewhat greater than SLJ-A3 strain value. This is in line with the tensile test results for adhesive specimens, which indicate that A3 has a very tiny modulus or is more likely to be ductile, whereas A1 has a greater elastic modulus. Although A3 is the weakest, it exhibits similar ductility to A1, whereas A1 offers a balance between strength and ductility. These results imply that the.

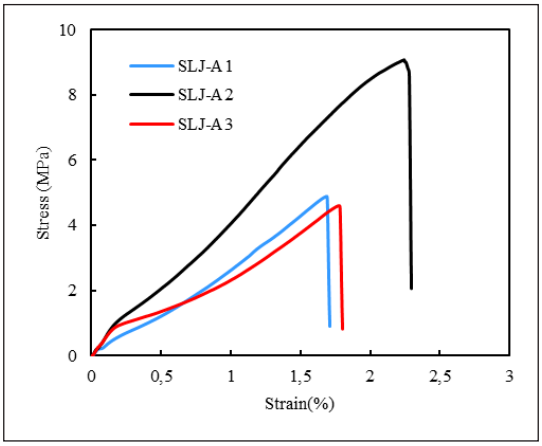


Figure 3.5: Stress-Strain Curve of SLJ Specimens.

3.4. Simulation

The SLJ simulation in this paper is only performed on SLJ-A2, which has the highest modulus of elasticity compared to SLJ-A1 and SLJ-A3. Since the adhesive simulation uses spring elements. The initial step involves calculating the forces in the x- and y-directions within the overlap region. The corresponding shear stresses are then obtained by dividing each force component by its respective area, as defined in Equation 2-2. The shear stress distribution in the single lap joint's adhesive layer can be obtained by this calculation. Then, the shear stress (in MPa) is plotted against the overlap area in the x and y directions (both in mm). The shear stress results obtained from FEA will be compared with the results from experimental testing. Ideally, if all parameters—such as the material properties of the adhesive, specimen geometry, and the applied load—are consistent between the FEA simulation and experimental testing, the results should closely match. However, if there is a significant discrepancy between the two results, it is essential to re-examine the parameters used to ensure they are correctly defined and accurately represented in both the simulation and the testing process.

Figure 3.6 presents the shear stress distribution across the adhesive layer of a single-lap joint. The highest shear stresses occur near the overlap edges in both the x- and y-directions, with peak values of approximately 13.8 MPa. Finite Element Analysis (FEA) reveals stress variations within the adhesive layer, in contrast to experimental testing, which typically yields only an average shear stress value calculated by dividing the applied load by the adhesive's cross-sectional area..

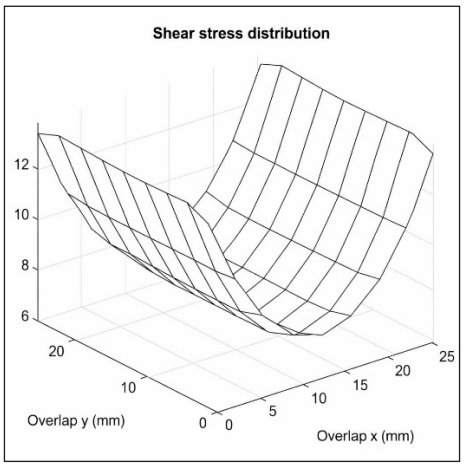


Figure 3.6: Shear stress profile in the SLJ adhesive layer.

The shear stress gradually decreases as the position shifts toward the center of the overlap area, forming a concave distribution profile. The central region exhibits the lowest shear stress, namely 7.06 MPa. This indicates that the adhesive in this area bears the smallest shear load. Based on the FEA results, the average shear stress is 9.82 MPa. Meanwhile, the theoretical value determined using a load of 6000 N and an overlap area of 25.4 × 25.4 mm is 9.30 MPa. The maximum value at the edge indicates a concentration of shear stress at the boundary of the adhesive layer. This concentration occurs due to a sudden transition in the overlap region, where the load is transferred through the adhesive at the edges. Along the length of the overlap (x-direction), the shear stress decreases from the maximum value at the edges to the minimum value at the center. This indicates that the load distribution is not uniform across the entire adhesive layer. Meanwhile, the shear stress across the width of the overlap (y-direction) tends to be constant, with only slight variations observed at the corners, as indicated by the lines below the graph.

High shear stress at the edges of the joint is a common characteristic of single-lap joints. This is because the adhesive near the joint boundary bears the greatest load during the loading process. Given that this region is more susceptible to failure, this can be a critical factor for the integrity of the joint. Low shear stress in the center of the overlap area indicates that the adhesive in this region is not being fully utilized in terms of its load-bearing capacity. This means that the center of the adhesive layer contributes less to the overall strength of the joint compared to its edges. The maximum shear stress at the edges and the minimum shear stress in the center highlight the need to ensure that the adhesive and joint design can withstand these stress concentrations to prevent premature failure.

Table 3-2 shows a comparison of the average shear stress results obtained from theoretical calculations, experimental tests, and FEA simulations. The standard value was obtained from theoretical calculations, namely 9.30 MPa, while the average shear stress values from the experiments and FEA simulations were 9.44 ± 0.28 MPa and 9.82 MPa, respectively. The percentage deviation from the theoretical value was 1.51% for the experimental results and 5.59% for the FEA results.

Table 3-2: Comparison of Average Shear Stress

A2 Model	Average Shear Stress (MPa)
Theory	9.30
Experiment	9.44
FEA	9.82

3.5. Failure Analysis

Single lap joint (SLJ) failure modes are classified according to ASTM D5573 (ASTM International, 1999). Single lap joint specimens using adhesive A2 show mixed failure modes, which combine adhesion and cohesion mechanisms, as evidenced by the failure analysis. As illustrated in Figure 3.7 (a), An adhesive failure, in which the glue has totally separated from one of the bonded materials while remaining connected to the other, is shown by the clean area on the bond surface.

This figure also illustrates a cohesive failure, evidenced by a crack in the adhesive that extends across nearly half of the overlap area. Figure 3.7 (b) shows a side view from the failure, where deformation in the bonded area indicates a strong bond between the adhesive and the bonded materials. The failure mechanism can be explained as follows: under continuous loading, the strong bond between the adhesive and the bonded objects, in combination with the continuous application of load, causes deformation in the bonded area. As the load exceeds the adhesive's bond strength, delamination begins at the edges of the joint, and the adhesive finally cracks near the center of the overlap area, being unable to withstand more load.

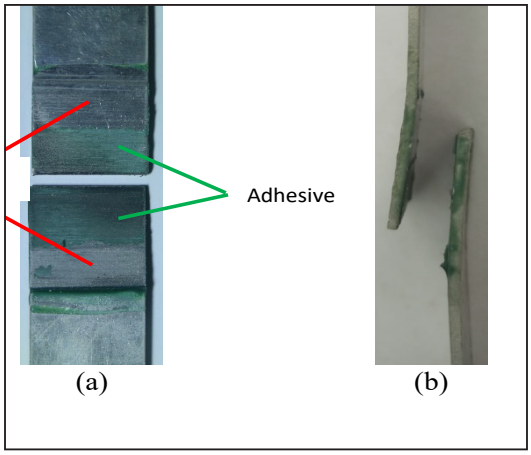


Figure 3.7: Failure in SLJ-A2 Specimens (a) Front View, (b) Side View.

The findings of the failure analysis of the SLJ-A1 single-lap adhesive joint with A1 adhesive are displayed in Figure 3.8, which reveals a combined adhesive and cohesive failure mode with features different from those of the SLJ-A2 specimen. The region of adhesive failure is much bigger than that seen in SLJ-A2, and the failure zones are more widely distributed, as shown in Figure 3.8 (a). Additionally, Figure 3.8 (b) demonstrates that, in contrast to the SLJ-A2 specimen, the SLJ-A1 specimen displays no discernible deformation. The lack of deformations suggests that SLJ-A1's shear strength is lower than SLJ-A2's and points to a distinct failure process. These variations in failure modes show that the adhesive's characteristics significantly affect the joint's overall performance.

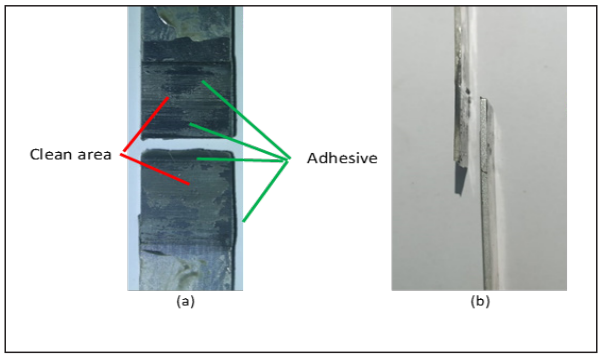


Figure 3.8: Failure in SLJ-A1 Specimens (a) Front View, (b) Side View.

The failure analysis of the single-layer adhesive joint (SLJ-A3) bonded with A3 reveals a mixed-mode failure that comprises cohesive and adhesive failure, as seen in Figure 3.9. It is not the same as the SLJ-A2 and SLJ-A1 specimens. The adhesive failure zone in SLJ-A3 appears to be significantly wider than that seen in SLJ-A2 and SLJ-A1, as seen in Figure 3.9 (a). The middle of the bonded region contains this large area of adhesive failure, which is distinguished by the bonded items' clean surfaces and the lack of adhesive debris along the bonded area's margins. Figure 3.9 (b) demonstrates that, in contrast to the deformation shown in the SLJ-A2 specimen, the SLJ-A3 specimen displays no deformation, just like the SLJ-A1 specimen. The shear strength of SLJ-A3 is lower than that of adhesives SLJ-A2 and SLJ-A1, according to these observations, highlighting the impact of adhesive type on failure behavior and adhesive junction strength.

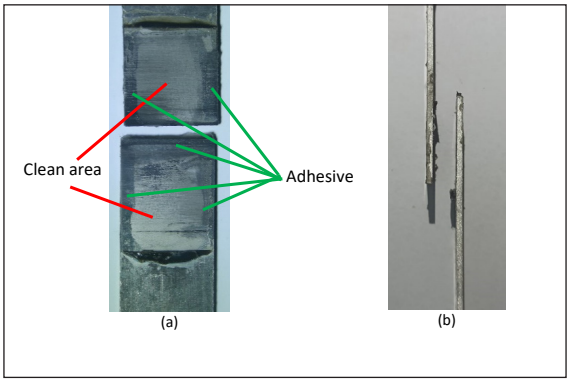


Figure 3.9: Failure in SLJ-A3 Specimens (a) Front View, (b) Side View.

The observed variations in failure modes in the SLJ specimens bonded with these adhesives are likely influenced by several factors. First, differences in the adhesive base material composition—where A1 and A2 are epoxy-based while A3 is based on acrylic—play a significant role. In addition, the properties of the adhesives, such as viscosity and other characteristics, differ among the trio. In particular, A2 exhibits the lowest viscosity, allowing for more even distribution of the adhesive during application, which contributes to a different failure mechanism compared to the other adhesives.

The experimentally observed failure modes show strong agreement with the stress distribution predicted by the finite element model. The FEA results revealed that the maximum shear stress was concentrated at the overlap edges, reaching approximately 13.8 MPa, while the central region experienced significantly lower stress levels. This non-uniform stress distribution indicates that the overlap edges are the most critical regions for load transfer and are therefore more susceptible to failure initiation.

The failure observations of the SLJ-A2 specimens supports this prediction. The presence of adhesive failure regions near the overlap boundaries suggests that crack initiation occurred at the joint edges, where the stress concentration is highest. In addition, the significant cohesive failure observed across a large portion of the overlap area indicates that once crack initiation occurred at the edges, the crack propagated through the adhesive layer under continued loading. The visible deformation of the bonding area further confirms the presence of bending and peel effects, which are characteristic of single-lap joints and are implicitly captured by the numerical model.

4. Conclusions

This study evaluates the performance of three types of adhesives—two aerospace-grade adhesives (3M™ Scotch-Weld™ EC-2216 B/ A and Araldite® 420A)—on single-lap aluminum joints through experimental testing, numerical simulation, and failure analysis. At the overlap, Araldite® 420A shows the highest tensile strength, modulus of elasticity, and shear strength, suggesting better stiffness and load-bearing capacity. With a variation of less than 6%, FEA verified the existence of stress concentrations at the overlap edges, which is in line with theoretical predictions and experimental findings. In contrast to other adhesives that displayed more extensive areas of adhesive failure, the failure study shows that Araldite® 420A mostly displays cohesive failure, indicating stronger adhesion to the aluminum substrate. For aerospace-grade aluminum joints, Araldite® 420A was found to be the best adhesive overall. However, because the testing was done at ambient temperature, this study had limitations. There could only be one overlap in the overlap geometry. There were quasi-static loading conditions. It is anticipated that subsequent studies will.

5. Acknowledgements

This research is funded by National Research and Innovation Agency under Grant No. 1/III.1/HK/2025.

6. Contributor Statement

The authors have read and approved the final manuscript. The authors have contributed meaningfully to the development and design of this research. The authors are responsible for data collection, analysis, and interpretation of the results.

7. References

Abdurohman, K., Pratomo, R. A., Hidayat, R., Ramadhan, R. A., Nurtiasto, T. S., Ardiansyah, R., … Wandono, F. A. (2024). Influence of Abrasion Treatments on Performance of Adhesively Bonded Glass/Vinyl Ester Single Lap Joints. *Evergreen*, *11*(2), 806–820. https://doi.org/10.5109/7183361

Akpinar, S., Doru, M. O., Özel, A., Aydin, M. D., & Jahanpasand, H. G. (2013). The effect of the spew fillet on an adhesively bonded single-lap joint subjected to bending moment. *Composites Part B: Engineering*, *55*, 55–64. https://doi.org/10.1016/j.compositesb.2013.05.056

Andarabi, A. A., Shelesh-Nezhad, K., & Chakherlou, T. N. (2022). The effect of laser surface structuring patterns on the interfacial resistance of aluminum joints bonded with epoxy adhesive. *International Journal of Adhesion and Adhesives*, *114*. https://doi.org/10.1016/j.ijadhadh.2022.103101

ASTM International. (2014). *Standard Test Method for Tensile Properties of Plastics (ASTM D638-14)*. West Conshohocken, PA: ASTM International. https://doi.org/10.1520/D0638-14

Boutar, Y., Naïmi, S., Mezlini, S., & Ali, M. B. S. (2016). Effect of surface treatment on the shear strength of aluminium adhesive single-lap joints for automotive applications. *International Journal of Adhesion and Adhesives*, *67*, 38–43. https://doi.org/10.1016/j.ijadhadh.2015.12.023

Cui, X., Tian, L., Wang, D. S., & Dong, J. P. (2021). Summary of thermosetting composite material welding. *Journal of Physics: Conference Series*, *1765*(1). IOP Publishing Ltd. https://doi.org/10.1088/1742-6596/1765/1/012021

Dachev, D., Kazilas, M., Alfano, G., & Omairey, S. (2025, June 1). Towards Reliable Adhesive Bonding: A Comprehensive Review of Mechanisms, Defects, and Design Considerations. *Materials*, Vol. 18. Multidisciplinary Digital Publishing Institute (MDPI). https://doi.org/10.3390/ma18122724

Demiral, M. (2025). Strength in Adhesion: A Multi-Mechanics Review Covering Tensile, Shear, Fracture, Fatigue, Creep, and Impact Behavior of Polymer Bonding in Composites. *Polymers*, *17*(19), 2600. https://doi.org/10.3390/polym17192600

Guo, C., Chen, Y., Zhang, H., Ji, H. P., Wu, Z., Liu, X., & Nagaumi, H. (2023). Synchronous improvement of mechanical properties and corrosion resistance of novel heat-treatable 5xxx aluminum alloy by non-isothermal ageing. *Journal of Alloys and Compounds*, *939*. https://doi.org/10.1016/j.jallcom.2023.168770

Guo, L., Liu, J., Xia, H., Li, X., Zhang, X., & Yang, H. (2021). Effects of surface treatment and adhesive thickness on the shear strength of precision bonded joints. *Polymer Testing*, *94*. https://doi.org/10.1016/j.polymertesting.2021.107063

Hecht, M., Fass, M., & Baumgartner, J. (2023). Fatigue strength of adhesively bonded deep drawn sheet specimens under multiaxial loading with variable amplitudes. *Procedia Structural Integrity*, *57*, 581–588. Elsevier B.V. https://doi.org/10.1016/j.prostr.2024.03.064

Maggiore, S., Banea, M. D., Stagnaro, P., & Luciano, G. (2021). A Review of Structural Adhesive Joints in Hybrid Joining Processes. *Polymers*, *13*(22). https://doi.org/10.3390/polym13223961

Marchione, F. (2020). Investigation of vibration modes of double-lap adhesive joints: Effect of slot. *International Journal of Engineering, Transactions A: Basics*, *33*(10), 1917–1923. https://doi.org/10.5829/IJE.2020.33.10A.10

Marchione, F. (2023). Shear Stress Distribution in Double-lap Adhesive Joints Reinforced with Nylon Fabric: Numerical Investigation. *International Journal of Engineering, Transactions A: Basics*, *36*(1), 35–40. https://doi.org/10.5829/ije.2023.36.01a.05

Miturska-Barańska, I., & Rudawska, A. (2022). Influence of Adhesive Compound Viscosity on the Strength Properties of 1.0503 Steel Sheets Adhesive Joints. *Advances in Science and Technology Research Journal*, *16*(2), 196–205. https://doi.org/10.12913/22998624/147314

Moazzami, M., Akhavan-Safar, A., Ayatollahi, M. R., Poulis, J. A., da Silva, L. F. M., & Teixeira De Freitas, S. (2023). A degradable mode I cohesive zone model developed for damage and fracture analysis of dissimilar composite/metal adhesive joints subjected to cyclic ageing conditions. *Theoretical and Applied Fracture Mechanics*, *127*. https://doi.org/10.1016/j.tafmec.2023.104076

Paz, E., Narbón, J. J., Abenojar, J., Cledera, M., & del Real, J. C. (2016, November 1). Influence of Acrylic Adhesive Viscosity and Surface Roughness on the Properties of Adhesive Joint. *Journal of Adhesion*, Vol. 92, pp. 877–891. Taylor and Francis Inc. https://doi.org/10.1080/00218464.2015.1051221

Rahul, B., Suresh, C., Narendran, E., & Haribaskar, R. (2023). Mechanical Characterization of Adhesive in Lap Joint Under Tensile Load. *Journal of Polymer & Composite*, (13). https://doi.org/10.37591/JoPC

Ramaswamy, K., O'Higgins, R. M., Kadiyala, A. K., McCarthy, M. A., & McCarthy, C. T. (2020). Evaluation of grit-blasting as a pre-treatment for carbon-fibre thermoplastic composite to aluminium bonded joints tested at static and dynamic loading rates. *Composites Part B: Engineering*, *185*. https://doi.org/10.1016/j.compositesb.2020.107765

Tahmasebi, F. (2002). Automation Tools for Finite Element Analysis of Adhesively Bonded Joints. *JSME/ASME International Conference on Materials and Processing*. Honolulu, USA: The Japan Society of Mechanical Engineers.

Teixeira de Freitas, S., & Sinke, J. (2015). Failure analysis of adhesively-bonded skin-to-stiffener joints: Metal-metal vs. composite-metal. *Engineering Failure Analysis*, *56*, 2–13. https://doi.org/10.1016/j.engfailanal.2015.05.023

Vinay, M. N. (2021). Optimization of adhesive bonding parameters of aluminium 6082 joints. *AIP Conference Proceedings*, *2317*. American Institute of Physics Inc. https://doi.org/10.1063/5.0036127

Wei, Y., Jin, X., Luo, Q., Li, Q., & Sun, G. (2024). Adhesively bonded joints – A review on design, manufacturing, experiments, modeling and challenges. *Composites Part B: Engineering*, *276*. https://doi.org/10.1016/j.compositesb.2024.111225

Wu, Y., Lin, J., Carlson, B. E., Lu, P., Balogh, M. P., Irish, N. P., & Mei, Y. (2016). Effect of laser ablation surface treatment on performance of adhesive-bonded aluminum alloys. *Surface and Coatings Technology*, *304*, 340–347. https://doi.org/10.1016/j.surfcoat.2016.04.051

Zhang, D., & Huang, Y. (2021). Influence of surface roughness and bondline thickness on the bonding performance of epoxy adhesive joints on mild steel substrates. *Progress in Organic Coatings*, *153*. https://doi.org/10.1016/j.porgcoat.2021.106135

Zhang, R., Li, J., Li, Q., Qi, Y., Zeng, Z., Qiu, Y., … Birbilis, N. (2019). Analysing the degree of sensitisation in 5xxx series aluminium alloys using artificial neural networks: A tool for alloy design. *Corrosion Science*, *150*, 268–278. https://doi.org/10.1016/j.corsci.2019.02.003